energy&fuels

Article

Cite This: Energy Fuels 2019, 33, 7726−7737

pubs.acs.org/EF

Catalytic Study of Hexadecane Cracking over Novel and Efficient HY/Al-HMS/K10 Hybrid Catalysts

Sara Masoudinejad and Vahid Mahdavi*

Department of Chemistry, Surface Chemistry and Catalysis Division, Faculty of Sciences, Arak University, Arak 38156-8-8349, Iran

ABSTRACT: The aim of this study is to provide a new and high-performance catalytic system for the cracking process by combining HY-zeolite, Al-hexagonal mesoporous molecular sieves (HMS) as a new matrix, and montmorillonite K10 as filler components. The Al-HMS molecular sieve was synthesized with different Si/Al molar ratios in the range of 2.5−35 and assembled with various amounts of HY-zeolite and montmorillonite K10 to prepare two- and three-component catalysts. After calcination, their catalytic activities were investigated in a cracking reaction of *n*-hexadecane at 500 °C and atmospheric pressure as a model reactant. The structure and surface properties of the synthesized catalysts were characterized by X-ray diffraction, scanning electron microscopy, Brunauer−Emmett−Teller, temperature-programmed desorption of NH_3, and pyridine-IR techniques. Results indicated that the desired hybrid catalysts were successfully synthesized with the micro-mesoporous structures, high surface area, and suitable pore volume, and their performance was directly related to the strength of Lewis and Brønsted acid sites as well as the ratio of microporous−mesoporous structures. The optimized ZAK(35) catalyst (containing 35 wt % NH_4Y, 50 wt % K10, 15 wt % Al-HMS(5), and Si/Al molar ratio of 5 in matrix) with proper textural properties, appropriate ratio of mesopore to microspore structure, suitable thermal stability to about 750 °C, and a higher Brönsted/Lewis acid sites ratio exhibited an excellent ability in the cracking of *n*-hexadecane. In optimum condition over the ZAK(35) catalyst, *n*-hexadecane conversion of 69% was achieved, and the selectivity values of gasoline, liquefied petroleum gas, and dry gas were 71, 20, and 4.5%, respectively.

1. INTRODUCTION

The catalytic cracking of hydrocarbons in a fluid-bed process [fluid catalytic cracking (FCC)] is one of the most important processes of the petroleum industry for producing diesel fuel and high-octane gasoline from heavy crude oil.[1] In recent years, demand for gasoline and light gases has increased, which has led to the development and improvement of cracking units in the conversion of heavy crude oils to gasoline.[2] Commercial fluid cracking catalysts are composed of several components that are providing the best efficiency to break down heavy feedstock into gasoline. Cracking process catalysts are typically composed of active matrixes, crystalline Y-zeolite, filler materials, and other additives.[3−8] Zeolite used in the structure of cracking catalysts is a synthetic, faujasite-type Y-zeolite and high in silica type, which has a significant effect on the activity and selectivity of the FCC catalyst.[9]

Zeolite materials have a microporous structure, which is constructed from the combination of SiO_4 and AlO_4 tetrahedral units. These materials have been widely applied in catalysts as well as in separation and purification processes due to their regular porous structures, high thermal resistance, and high surface areas.[10−13] Several studies have investigated the acidity and structural properties of zeolite.[14−20] In general, the pore size and acidity of zeolite are modified to minimize coke formation and to maximize the selectivity to light fuel. In fact, strong acidic sites are needed to initiate the cracking process, and special characters of pore structures are needed to limit the coke formation.[21] The activity of zeolite in the cracking process is dependent on Brønsted acidic sites because the cracking reaction of hydrocarbons is carried out via formation of carbaniun ion intermediate.[1,4,22,23] Also, the zeolites are widely used in hydrocarbon isomerization, hydrocracking, reforming, and alkylation processes as heterogeneous catalysts.[24]

The matrix materials display a significant role in enhancing the performance of cracking process catalysts.[25] By loading the active matrix, such as alumina, aluminasilicates, and mesoporous silicas in the round of zeolite, especially when heavy oil is used as a feed, the large molecules can be precracked into moderate molecules. These molecules can then diffuse into zeolite pores and convert into smaller molecules with appropriate selectivity.[26−28] Also, the uniform distribution of active zeolite and matrix sites and the relationship between different pore structures have an important effect on the textural properties and acidic strength and, consequently, on the catalyst performance.[29] Much research has been conducted to discover the relationship between the matrix and zeolite.[30−35] In 1992, a mesoporous MCM-41 molecular sieve was discovered by Mobil Company and used as a matrix in FCC catalysts.[36,37]

Studies on the performance of FCC catalysts have shown that catalytic activity increases with increasing matrix acidity, but at the same time the value of coke formation also increases. Therefore, the acidity of the matrix in the cracking catalyst should be adjusted at the appropriate level.[3,4,6] In fact, the precracking of heavy feed was carried out on the meso- or macropores of the matrix, and then the produced molecules with small molecular weights diffused into the microporous zeolite pores and cracked to the target products.[38]

Received: May 22, 2019
Revised: July 22, 2019
Published: August 6, 2019

DOI: 10.1021/acs.energyfuels.9b01649
Energy Fuels 2019, 33, 7726−7737

In several papers, the hexagonal mesoporous molecular sieves (HMS) with a wormlike pore structure have been used in partial oxidation,[39,40] hydrogenation,[41] and carbonylation[42] processes as support in heterogeneous catalysts. Several catalysts have also been prepared by incorporation of various heteroatoms such as Al, Ga, Fe, Ti, Zr, Co, and V into the HMS framework.[43−47] It has been made clear that aluminum substitution into the HMS structure (Al-HMS) will increase the Brönsted acidity satisfactorily. Chiranjeevi et al. reported synthesis of Al-HMS molecular sieves and investigated their activities for the cumene cracking reaction.[48] Hamoule et al. used Pt/Al-HMS catalysts for *n*-heptane reforming,[49] Kulikov et al. studied the oligomerization of α-olefins over Al-HMS and Al-MCF catalysts,[50] and Onaka et al. investigated the Diels−Alder reaction of acrylates with 1,3-dienes over solid acid sites of the Al-HMS catalyst.[51]

These mesoporous materials (HMS, Al-HMS) with high surface area, excellent thermal stability, and moderate acidity can be used as a matrix in FCC catalysts. According to literature review, the applications of HMS and Al-HMS have not been reported as a matrix in cracking catalysts. Therefore, in this study, for the first time, the new cracking catalysts were synthesized by using Y-zeolite, Al-HMS, as a matrix and montmorillonite (K10) as a filler and applied for cracking of hexadecane as a model reaction. The purpose of this study is to develop a catalytic system in this area and to provide a new and high-performance catalytic system for the cracking process. The combination of HY-zeolite, Al-HMS, as new matrix and montmorillonite K10 as filler components has not been reported, and the details of the effective parameters in this catalytic system should be investigated. In this way, the catalyst activity in the cracking reaction will be enhanced by creating a good ratio of strong and medium acid sites, as well as a good ratio of micro- and mesoporous structures. The texture and surface properties of the catalyst samples were characterized by scanning electron microscopy (SEM), Brunauer−Emmett−Teller (BET) isotherm, powder X-ray diffraction (XRD), temperature-programmed desorption of NH_3 (TPD-NH_3), and Fourier transform infrared (FTIR) spectra of adsorbed pyridine.

2. EXPERIMENTAL SECTION

2.1. Materials. $NaAlO_2$ (containing Al_2O_3 52.82 wt % and Na_2O 40.24 wt %) and Na_2SiO_3 materials were purchased from Alfa-Aesar Company.

$C_9H_{22}AlO_3$ (aluminum isopropoxide), $C_8H_{20}O_4Si$ [tetraethyl orthosilicate (TEOS)], $C_{12}H_{27}N$ [dodecylamine (DDA)], NaOH, NH_4NO_3, isopropyl alcohol (IPA), and ethanol were purchased from Merck Company. Montmorillonite K10 was purchased from Fluka, and $C_{16}H_{34}$ (*n*-hexadecane) as feed was purchased from Sigma-Aldrich company.

2.2. Catalyst Preparation. *2.2.1. Preparation of NaY and NH_4Y Zeolite Powder.* To synthesize 3 g of NaY-zeolite, the seed gel was first prepared according to the following procedure: 1.95 g of deionized water and 0.4 g of sodium hydroxide with 0.2 g of sodium aluminate were stirred in a plastic bottle until dissolved, and then 2.27 g of sodium silicate solution was added to the previous mixture and stirred moderately. After stirring, the plastic beaker was covered, and the solution was allowed to age at room temperature for 24 h. Then, the feedstock gel was prepared as follows: 13.09 g of deionized water, 0.014 g of sodium hydroxide, and 1.30 g of sodium aluminate were mixed in a plastic bottle, and then 14.2 g of sodium silicate solution was added to them and stirred vigorously until a smooth gel appears. For preparation of the final gel or overall gel, the seed gel was slowly added to the feedstock gel under high shear up to 20 min. The prepared overall gel with a molar composition of 4.62 Na_2O/1 Al_2O_3/10 SiO_2/180 H_2O was transferred to an autoclave container and was allowed to age at room temperature for 24 h; then, it was crystallized at 100 °C for 5 h. After this step, the gel was deposited in the solid form (containing the NaY-zeolite) at the bottom of the container. The wet solid product was filtered, washed with distilled water until the pH of the filtrate was below 9, and dried at 100 °C overnight.[52] To prepare NH_4-Y-zeolite, 30.0 mL of 1.5 M NH_4NO_3 aqueous solution with 1.0 g of the NaY-zeolite was mixed and then refluxed at 80 °C three times; each run time was 3 h. Then, the precipitate was filtered, washed with distilled water, and dried at 100 °C overnight.

2.2.2. Preparation of HMS and Al-HMS with Different Si/Al Molar Ratios. The HMS and Al-HMS materials were synthesized by the sol−gel method according to the procedure by Pinnavaia and co-workers.[53] Mokaya and Jones[54] used tetraethyl orthosilicate (TEOS) as the silica source, aluminum isopropoxide as the aluminum source, and dodecylamine (DDA) as the surfactant. In a typical synthesis of Al-HMS(35) (Si/Al = 35), 0.55 g of aluminum isopropoxide was mixed with 20 mL of isopropyl alcohol (IPA) (solution A). Then, 4.55 g of dodecylamine was also mixed with 59.8 g of water and 1.82 mL of HCl 1 N and was stirred for 15 min (solution B). On the other hand, 19.5 g of TEOS was added to 27.3 g of ethanol and stirred for 30 min (solution C). Then, solution A was added to solution B and stirred for 30 min, and then this solution was mixed with solution C and stirred moderately for 44 h to obtain the solid crystalline product. The solid white product was separated by a vacuum pump, dried at 110 °C overnight, and calcined at 600 °C for 5 h in air with temperature programming. The pure HMS was also synthesized using the same method as above but without using solution A. The materials with different Si/Al molar ratios were prepared by applying proper values of aluminum isopropoxide and TEOS to obtain 2.5, 5, 10, 20, and 35 Si/Al molar ratios following the above procedure and were named Al-HMS(x), where x represents the Si/Al molar ratio.

2.2.3. Preparation of Al-HMS/HY Catalysts. To prepare two-component Al-HMS/HY catalysts, each of the samples Al-HMS(x) (x = 2.5, 5, 10, 20, and 35) were mixed with zeolite HY in an equal weight ratio; then, enough water was added to them and placed in an ultrasonic bath for 1 h. The resulting mixtures were stirred at 60 °C to form a paste mixture and dried at 100 °C overnight. These samples were named NH_4Y/Al-HMS(x) or briefly ZA(x), where x represents the Si/Al molar ratio. The ZA(x) catalyst samples were in situ calcined at 550 °C under dry airflow for 3 h before the catalytic test.

2.2.4. Preparation of NH_4Y/Al-HMS(5)/K10 Catalysts with Different Weight Ratios. These three-component catalyst samples were prepared by mixing 50 wt % clay montmorillonite K10 as the filler and x wt % NH_4Y-zeolite and y wt % Al-HMS(5) (with molar ratio of Si/Al = 5) as the matrix, so that the sum of x and y was constant (50 wt %). The samples were prepared with different weight percentages of zeolite and matrix (x = 15, 25, and 35 wt %) well mixed; then, the appropriate amount of water was added to them and placed in an ultrasonic bath for 2 h. Then, these samples were stirred well at 60 °C to achieve a dough mixture. The resulting mixtures were dried at 100 °C overnight. These samples were named NH_4Y(x)/Al-HMS(5)/K10 or briefly ZAK(x), where x represents the weight percentage of NH_4Y-zeolite. The ZAK(x) catalyst samples were in situ calcined at 550 °C under dry airflow for 3 h before the catalytic test.

2.3. Catalyst Characterization. The crystalline structures of the hybrid catalysts and the component were determined by powder X-ray diffraction (XRD) by a STOE diffractometer with Cu Kα (λ = 0.15406 nm) radiation and a Ni filter. The diffractogram was recorded in the range of 2θ = 1−80° with a scanning rate of 2° min^{-1}. The Si(111) XRD pattern was used as an external standard for calibration of XRD peak positions, and crystalline phases of the catalyst samples were identified by comparing with the JCPDS reference data pattern.

To investigate the morphology and particle size of the catalyst samples, the field emission scanning electron microscopy (SEM) images coupled with energy-dispersive spectroscopy (EDS) were recorded by a MIRA3TESCAN-XMU instrument. Nitrogen adsorption−desorption isotherms at 77 K were recorded on a Micromeritics

DOI: 10.1021/acs.energyfuels.9b01649
Energy Fuels 2019, 33, 7726−7737

ASAP 2010 instrument. Before the measurements, catalyst samples were degassed for 5 h at 200 °C. The Barrett−Joyner−Halenda (BJH) algorithm was also used for calculating the average pore diameter (d_p). The specific surface area is determined from adsorption data by the BET theory, and the total pore volume is estimated from the amount adsorbed at a p/p_0 = 0.99.

The acidity of the catalyst samples was evaluated by ammonia temperature-programmed desorption (NH_3-TPD) experiments using a Micromeritics AutoChem 2920 chemisorption analyzer. Next, 60 mg of the catalyst sample was placed in a quartz reactor, and it was degassed by passing a N_2 stream (30 mL min^{-1}) at 350 °C for 1.5 h and cooled down to 110 °C. The NH_3 chemisorption was subsequently performed by the adsorption of 5% NH_3/He with a flow rate of 50 mL min^{-1} at 110 °C for 40 min. The physisorbed ammonia was then removed from the surface of the catalyst by a helium stream (30 mL min^{-1}) for 40 min at 110 °C. Then, the samples were heated again from 110 to 900 °C at a heating rate of 10 °C min^{-1} in a flow of He (30 mL min^{-1}), and NH_3 desorption was detected by a thermal conductivity detector (TCD) using a Shimadzu gas chromatograph (GC) (model 6A) instrument.

The Shimadzu spectrometer (model 8300) was used to record the FTIR spectra of adsorbed pyridine. The catalyst samples were heated at 400 °C under vacuum for 3 h, and then adsorption of purified pyridine vapor was performed at 100 °C for 30 min. Then, the samples were evacuated for desorption of physically adsorbed pyridine, and the pyridine-IR spectra were recorded by a spectrometer. To determine the amount of coke deposited on the surface of catalysts, the coke analyzer LECO induction furnace instrument model HF-400 was used.

2.4. Catalytic Tests and Calculation Methods. *2.4.1. Activity Evaluation.* Catalytic cracking reactions of *n*-hexadecane were performed at atmospheric pressure in a fixed-bed stainless steel reactor with 0.9 cm internal diameter and 50 cm length, which has already been described in a previous work.[55] The experimental setup is shown schematically in Figure 1. In a typical experiment, 1.0 g of

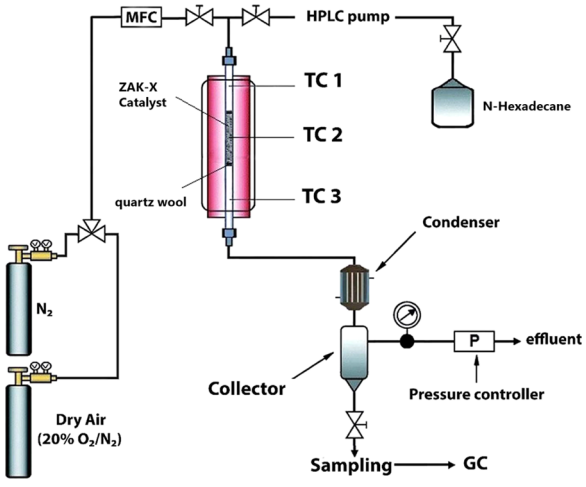

Figure 1. Schematic of the experimental setup fixed-bed reactor applied for the cracking reaction.

catalyst (30−50 mesh) and 3.0 g of corundum (50−70 mesh) were loaded separately in the middle section of the reactor, with quartz wool packed in both ends; subsequently, this sample was in situ activated at 550 °C under a 40 mL min^{-1} flow of dry air for 3 h. This process converts the zeolite in the catalyst sample from NH_4-Y into HY-zeolite form.[22] The temperature was then reduced to 500 °C and remained constant, and air was replaced with nitrogen gas. Thereafter, *n*-hexadecane was fed into the reactor by a peristaltic pump BT100-1F model at a rate of 4.7 mL h^{-1} along with N_2 carrier gas (140 mL min^{-1}). The mass flow controller (Brooks) was used to adjust the flow of carrier gas (N_2). Three thermocouples (TC 1−3) were inserted in the middle of the reactor to monitor the reaction temperature. The run time of each reaction was 40 min. The gaseous products were analyzed online using Varian GC 3800 equipped with a thermal conductivity detector (TCD) following a 2.5 m-long 1/8 in.-diameter Porapak Q (100−120 mesh) column. At the end of reaction, the liquid products were separated through ice water bathing and analyzed by a Dani gas chromatograph (GC) equipped with a flame ionization detector (FID) and a cpcill pona 7530 column. Conversion percentage was calculated based on the mole percentage of converted *n*-hexadecane. The conversion (%), selectivity (%), product yield (%), and carbon balance were calculated as follows:

$$\text{conversion (\%)} = (\text{moles of } n\text{-hexadecane reacted/moles of } n\text{-hexadecane in the feed}) \times 100 \quad (1)$$

$$\text{product selectivity (\%)} = (\text{moles of } n\text{-hexadecane converted to each product/mole of } n\text{-hexadecane reacted}) \times 100 \quad (2)$$

$$\text{product yield (\%)} = (\text{conversion of } n\text{-hexadecane} \times \text{selectivity of each product})/100 \quad (3)$$

$$\text{carbon balance} = (\text{mol of } n\text{-hexadecane converted to all desired products/mol of } n\text{-hexadecane converted} \quad (4)$$

The moles of *n*-hexadecane converted were calculated from the sum of the mole of the dry gases ($CO-CO_2-C_1-C_2$), liquefied petroleum gas (LPG) (C_3-C_4), gasoline (C_5-C_{12}), and coke. Also, the weight percentage of coke in the catalyst sample was measured using a coke analyzer, and the mass balances (carbon balance) were determined around >96% for each run.

3. RESULTS AND DISCUSSION

3.1. Catalyst Characterization. Figure 2A shows the XRD patterns of synthesized Al-HMS samples (after calcination) with different Si/Al molar ratios that are in good conformity with the literature.[53,54] In all patterns, a wide reflection peak at a low angle represents a mesoporous lattice with hexagonal symmetry. From comparing these patterns, it can be concluded that by increasing the amount of aluminum in the samples, the intensity of the peaks has decreased and the peak width has increased, indicating that incorporation of Al into the structure of the molecular sieve would increase the disorder of the lattice.[49]

Figure 2B shows the wide-angle range XRD patterns of the synthesized samples: Al-HMS(5), zeolite Y, and hybrid catalysts (ZAK) with different zeolite and Al-HMS(5) contents after calcination. As shown in Figure 2B, the XRD pattern of Al-HMS(5) has a peak in the low angle (2θ = 2−5°) due to the hexagonal mesoporous array and has a broad diffraction line (2θ = 20−30°) due to the shapeless part of the HMS structure. The XRD patterns of the HY-zeolite sample were observed in the ranges 2θ = 5−10 and 20−30°, corresponding to faujasite-type zeolite Y, which perfectly agrees with the JCPDS powder diffraction pattern 43-0168. Also, Figure 2B shows the XRD patterns of hybrid catalyst samples synthesized from mixing of zeolite, Al-HMS(5) (matrix), and montmorillonite K10 (filler) components. These diffraction patterns include the peaks of both Al-HMS(5) and Y-zeolite components so that increasing the HY content in the composite samples results in decreasing the characteristic Al-HMS(5) peak intensity and increasing the broadening of this peak. Therefore, from Figure 2B, it can be concluded that the lattice disorder of matrix Al-HMS(5) was increased from interaction with the HY-zeolite component, but the zeolite

DOI: 10.1021/acs.energyfuels.9b01649
Energy Fuels 2019, 33, 7726−7737

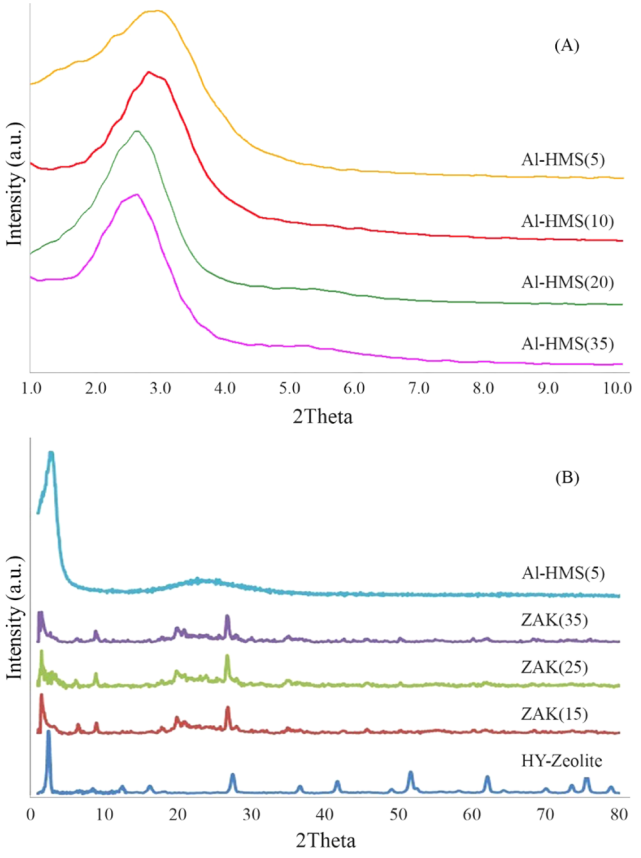

Figure 2. (A) Low-angle X-ray diffraction patterns of Al-HMS(x) samples with various molar ratios Si/Al 5, 10, 20, and 35 after calcination and (B) wide-angle XRD patterns of the synthesized samples: Al-HMS(5), zeolite Y, and hybrid catalysts ZAK(x) with different zeolite and Al-HMS(5) contents after calcination at 550 °C.

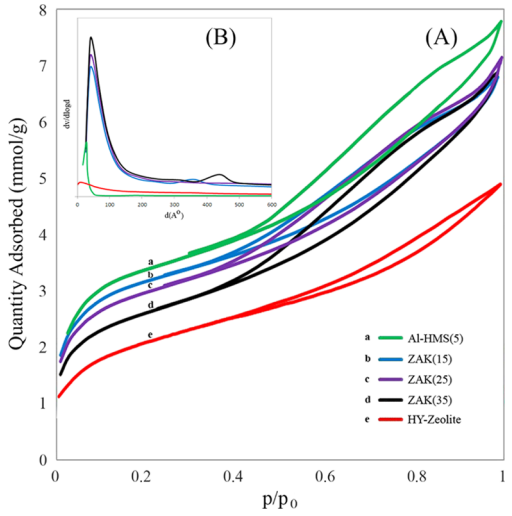

Figure 3. (A) N_2 adsorption−desorption isotherms at 77 K of Al-HMS(5), NH_4Y-zeolite, and ZAK(x) hybrid catalyst samples with 15, 25, and 35 wt % NH_4Y-zeolite after calcination at 550 °C and (B) BJH analysis of synthesized samples.

structure is almost preserved. Additionally, for three-component catalysts (ZAK(x)), however, the diffraction peaks for montmorillonite (K,10) are almost invisible due to their much lower intensity to those for Y-zeolite and Al-HMS(5). Table 1 shows the relative crystallinity (R.C.) parameters calculated from XRD patterns of the synthesized catalysts. It is clear from Table 1 that the crystallinity of the three-component hybrid catalysts has reduced compared with pure zeolite due to the presence of the Al-HMS matrix in the synthesized catalysts.

The pore structure properties of HY-zeolite, Al-HMS(5), and the hybrid catalyst ZAK(x) samples with different weight percentages of NH_4Y-zeolite(x) after calcination are characterized using the N_2 adsorption−desorption technique and presented in Figure 3A. The HY-zeolite sample (Figure 3A-e) clearly exhibited a standard type I isotherm with a clear hysteresis loop typical for microporous materials with sloping desorption and adsorption curves covering a wide range of p/p_0. In comparison, the Al-HMS(5) sample (Figure 3A-a) shows a mixture of type I and type IV isotherms due to mesoporous materials. The hybrid catalyst ZAK(x) samples (Figure 3A-b−d) displayed type I−IV isotherms and hysteresis loops that have characteristics of mesoporous materials with highly uniform cylindrical pores. In low-pressure ranges (p/p_0 < 0.2), the same trend is observed for hybrid catalysts. The textural characterization results of the synthesized catalysts are shown in Table 1.

The surface area of ZAK(x) hybrid catalysts reduced in comparison with pure components Al-HMS(5) and Y-zeolite due to the dense structure of the montmorillonite K10 used as the filler. As shown in Table 1, the surface area of the ZAK(x) catalyst varied from 254 to 210 $m^2\ g^{-1}$ depending on the weight percentage of NH_4Y-zeolite, and it decreases with the increase in NH_4Y-zeolite content. Also, the pore diameter values of ZAK(x) hybrid catalysts increased slightly with increasing zeolite content. A decrease in the total pore volume of the synthesized hybrid catalysts is as one would expect. By decreasing the S_{BET}, the total volume of nitrogen that can be adsorbed is also decreased. Also, Figure 3B shows the pore size distributions determined by the BJH method applying desorption branches of the N_2 isotherms. The values of pore size of these samples are shown in Table 1. The total pore volume was calculated from the mmol of adsorbed N_2 gas per gram catalyst at the relative pressure of 0.99. The micro- and

Table 1. Chemical and Textural Properties of the Catalyst Samples

catalysts	R.C.[a]	theoretical SAR	SAR[b]	S_{BET}[c] ($m^2\ g^{-1}$)	V_{micro}[d] ($cm^3\ g^{-1}$)	V_{total}[e] ($cm^3\ g^{-1}$)	$S_{external}$ ($m^2\ g^{-1}$)	pore size (Å)	V_{meso}[f] ($cm^3\ g^{-1}$)
ZAK(15)	35.2	4.1	4.3	254	0.024	0.23	161	39	0.206
ZAK(25)	45.5	3.5	3.6	239	0.038	0.23	151	43	0.192
ZAK(35)	58.2	2.9	3.1	210	0.042	0.23	154	49	0.188
Y-zeolite	100	2	1.9	304	0.140	0.14		8	
Al-HMS(5)		5	5.6	636		0.3	323	28	0.3

[a]Relative crystallinity calculated by X-ray diffraction analysis. [b]Molar ratio of Si/Al calculated from EDS analysis. [c]Calculated from the BET method. [d]Calculated from the t-plot method. [e]Volume adsorbed at p/p_0 = 0.99. [f]Calculated from $V_{meso} = V_{total} - V_{micro}$.

DOI: 10.1021/acs.energyfuels.9b01649
Energy Fuels 2019, 33, 7726−7737

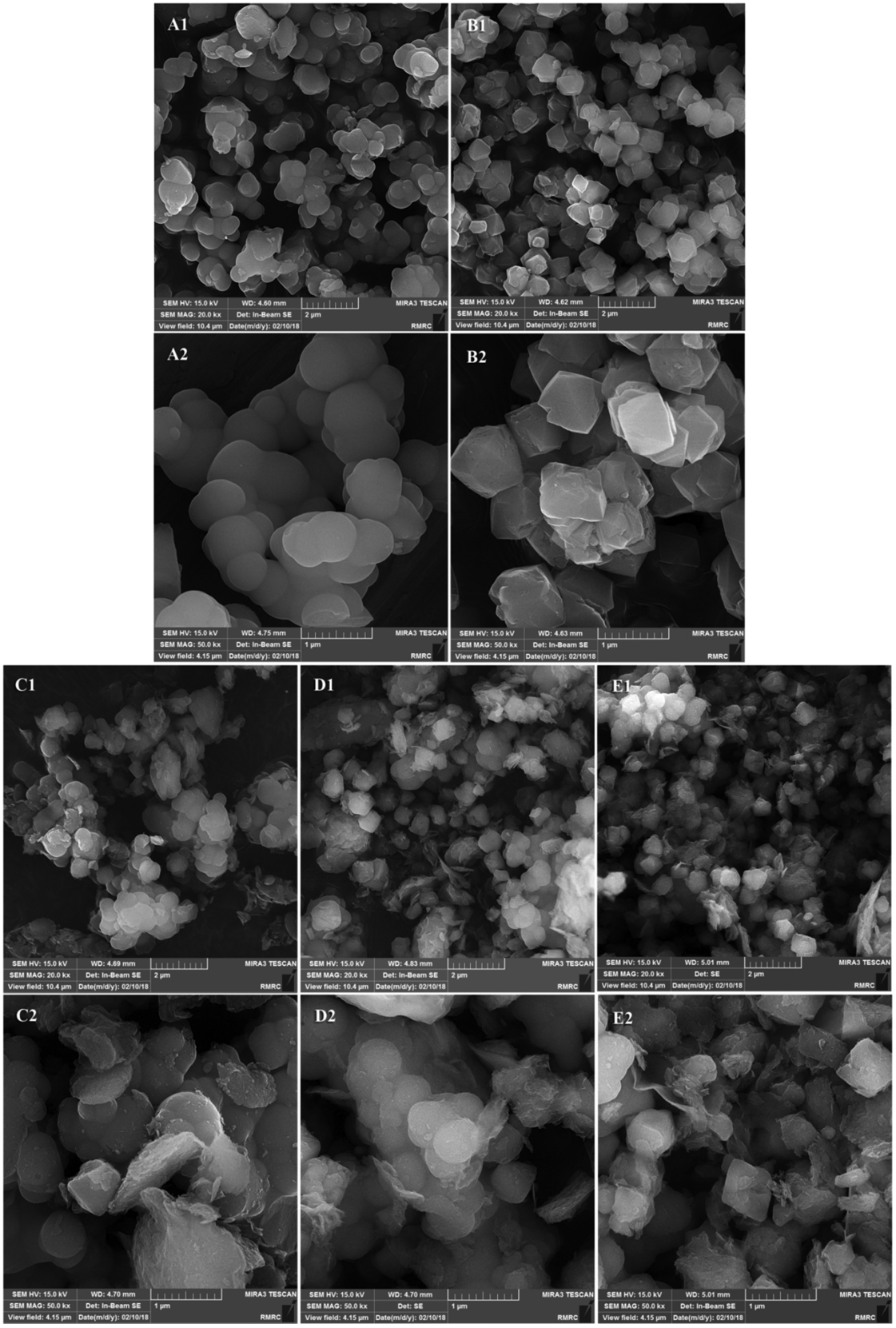

Figure 4. Scanning electron micrograph with two magnifications for Al-HMS(5) (A_1, A_2), NH_4Y-zeolite (B_1, B_2), and ZAK(x) hybrid catalyst samples (C_1, C_2, D_1, D_2, E_1, E_2) with 15, 25, and 35 wt % NH_4Y-zeolite after calcination at 550 °C.

mesopore volumes were calculated from the *t*-plot method and the $V_{meso} = V_{total} - V_{micro}$ equation, respectively. The values of these quantities are shown in Table 1. The presence of the mesoporous character in the structure of hybrid catalysts increases the external surface of the catalyst, making a larger number of pores accessible to the reactant molecules and

DOI: 10.1021/acs.energyfuels.9b01649
Energy Fuels 2019, 33, 7726−7737

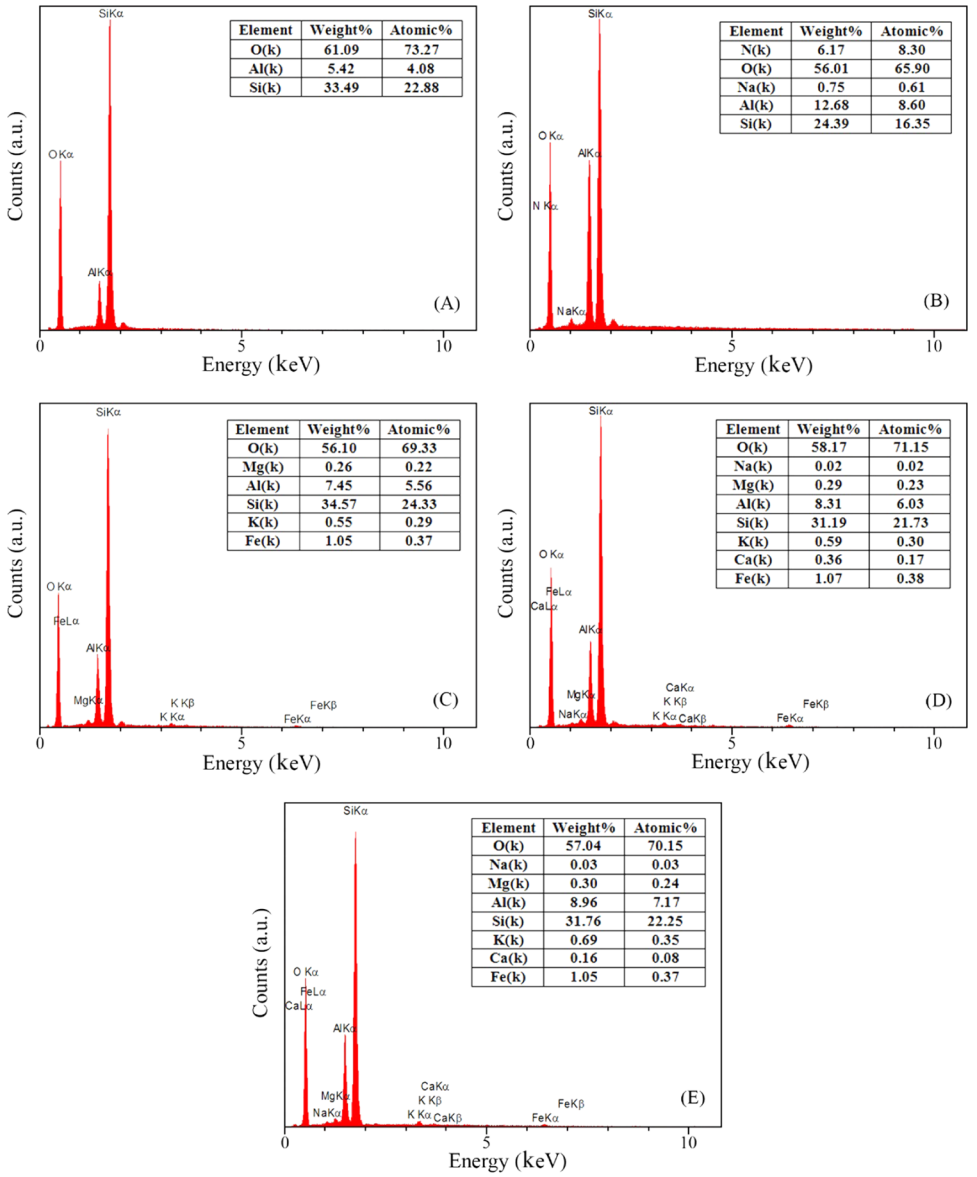

Figure 5. EDS analyses for (A) Al-HMS(5), (B) NH_4Y-zeolite, (C) ZAK(15), (D) ZAK(25), and (E) ZAK(35).

increasing the accessibility of the active sites of the catalyst inside the microporous channels. Therefore, this increases the diffusion rate of the products and reduces the rate of the formation of coke and dry gas.[56]

Figure 4 demonstrates SEM images of the Al-HMS(5), HY-zeolite, and ZAK(x) (x = 15, 25, 35) hybrid catalysts with different magnifications. The ZAK(x) hybrid catalyst has 50 wt % montmorillonite K10 as the filler and x wt % NH_4Y and 50 − x wt % Al-HMS(5) as a matrix. As shown in Figure 4A_1,A_2, the Al-HMS(5) sample is composed of small spherical crystals with size around 180−400 nm, and their external surfaces are flat and uniform. For the HY-zeolite sample (Figure 4B_1,B_2), the cubic morphology of the Y-zeolite was presented with all of the images, and the sizes of particles are around 500 nm, which represented that smaller crystals were agglomerated with the larger particles. The ZAK(x) hybrid catalysts showed both spherical and cubic morphologies of their constituents (Figure 4C_1,C_2 ZAK(15), D_1,D_2 ZAK(25), and E_1,E_2 ZAK(35)). In addition, the structure of the K10 filler shell is clearly visible in the images of this category of catalysts.

Figure 5 presents the X-ray electron-dispersive spectroscopy of pure Al-HMS, HY-zeolite, and ZAK(x) (x = 15, 25, 35) hybrid catalysts. Results indicate the presence of Al, O, and Si compositions in all of the synthesized samples. The weight percentage of the sodium ion is very small (0.02−0.75 wt %) in all samples of HY and ZAK(x) hybrid catalysts. Therefore, EDS analysis clearly shows that sodium ion exchange with a high percentage of ammonium ion was performed. The elemental analysis of the catalyst samples and Si/Al molar ratios determined by EDS analysis are summarized in Figure 5 and Table 1, respectively.

The NH_3-temperature programming desorption (NH_3-TPD) technique was applied for finding information about the amount and strength of the acidic sites present on the surface of synthesized catalysts. The amount of acidic sites is evaluated from the peak area, whereas the strength of acid sites is determined from the position and shape of peaks. Furthermore, according to the maximum temperature of the peak, in the NH_3-TPD curve, we can categorize acidic sites into weak, moderate, and strong.[56] The NH_3-TPD profiles of

DOI: 10.1021/acs.energyfuels.9b01649
Energy Fuels 2019, 33, 7726−7737

the Al-HMS(5), HY-zeolite components, and synthesized hybrid catalyst samples (ZAK(x)) after calcination are shown in Figure 6A,B, and the results are summarized in Table 2.

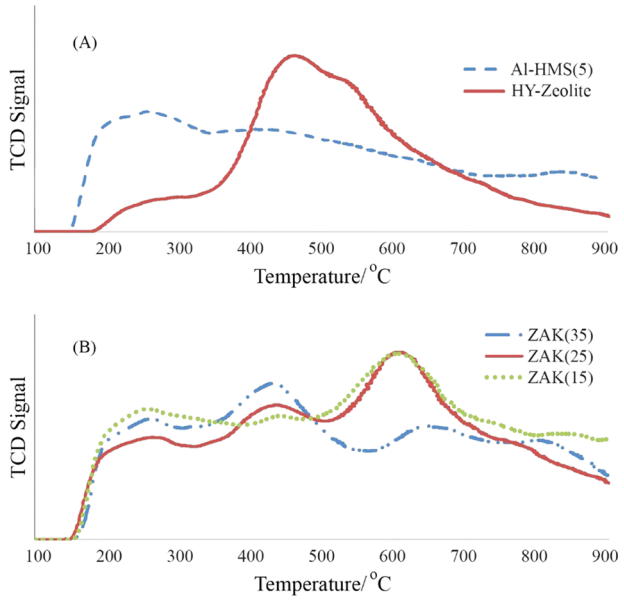

Figure 6. CO_2-TPD profiles of (A) Al-HMS(5), NH_4Y-zeolite, and (B) ZAK(x) hybrid catalyst samples with 15, 25, and 35 wt % NH_4Y-zeolite after calcination at 500 °C.

According to Figure 6A, the only NH_3 desorption peak on the Al-HMS(5) sample was in the range of 200−300 °C, which indicates the weak acid sites, whereas for the NH_4Y-zeolite sample after calcination there is one peak in the range of 400−700 °C corresponding to moderate to strong acid sites. According to Figure 6B, NH_3-TPD profiles of the synthesized catalyst samples (ZAK(x)) after calcination indicate three types of peaks. A peak in the range of 200−300 °C is related to weak acid sites, which is increased with the content of Al-HMS(5) in the ZAK(x) samples. The second peak in the range of 300−500 °C is related to moderate to strong acid sites, which depends on the zeolite content in the catalyst. However, the new peak that appeared in the range of 500−700 °C did not appear in any of the Al-HMS(5) and HY-zeolite samples individually. It can be related to the stronger acidic sites or superacidic character of the catalyst, generated from the interaction of catalyst components during the calcination process. This phenomenon may be related to the creation of Lewis acidic sites in the extra-framework of Al-containing species in the structure of ZAK(x) after calcination.[57] In fact, the strong acidic sites do not play a significant role in the cracking process, and the strong Lewis acids produce undesirable products such as coke; however, for cracking selectivity, weak Lewis acid sites and higher Brønsted acid sites are needed.[58] In other words, the strong acidic sites produced in the combined catalyst accelerate the start of the cracking process and then continue to route and produce the appropriate products on the moderate acid sites, so the catalyst with stronger acidity does not mean a better catalyst because more powerful sites produce more gas products and coke. Therefore, we expect that the ZAK(35) catalyst with a lower content of strong acidic sites is a desirable catalyst because it may produce less gas products and coke.

To evaluate the nature of acidic sites of the synthesized catalysts, pyridine adsorption coupled with FTIR analysis was considered. Figure 7 demonstrates the FTIR-pyridine spectra

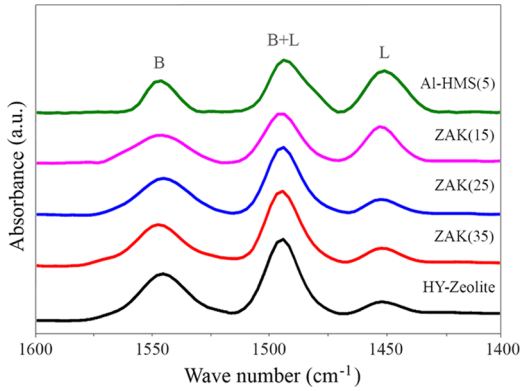

Figure 7. FTIR-pyridine spectra of Al-HMS(5), NH_4Y-zeolite, and ZAK(x) hybrid catalysts containing 15, 25, and 35 wt % NH_4Y-zeolite after calcination at 550 °C.

of the Al-HMS(5), NH_4Y-zeolite, and ZAK(x) hybrid catalyst samples. As shown in Figure 7, there are three absorption peaks in each catalyst spectrum graph. The peaks at 1545 and 1453 cm^{-1} were attributed to pyridine adsorbed on the Brönsted and Lewis acid sites, respectively.[59,60]

Furthermore, the intense band around 1490 cm^{-1} is attributed to the combination of Brønsted and Lewis (B + L) acid sites.[61] For HY-zeolite, the hydroxyl groups on the framework Si−O(H)−Al are the main source of the Brönsted acid site, whereas the Lewis acid sites are related to the Al^{3+} ion in the framework of zeolite.[1,23,62] Also, the blocking of the extra-framework aluminum species in the zeolite channel creates a little amount of Lewis acid sites.[63] For Al-HMS, Brönsted acid sites related to aluminum with tetrahedral coordination in the framework and octahedral extra-framework aluminums are the source of Lewis acid sites.[64−67] From Figure 7, it can be concluded that by increasing the proportion of zeolite in the ZAK(x) hybrid catalysts, the peak intensity of the

Table 2. Acidic Properties of the Synthesized Catalysts Evaluated from the NH_3-TPD Profile and FTIR-Pyridine Spectra

catalysts	total acidity[a] (μmol NH_3 g^{-1})	weak acid sites[a] (μmol NH_3 g^{-1})	moderate to strong acid sites[a] (μmol NH_3 g^{-1})	superacidic sites[a] (μmol NH_3 g^{-1})	(B/L) acid sites[b]
ZAK(15)	1175	312	183	679	0.56
ZAK(25)	1053	180	269	603	1.40
ZAK(35)	1002	172	409	421	2.42
Y-zeolite	994	82	912		9.40
Al-HMS(5)	1235	400	603		1.30

[a]The values of total acidity were calculated by means of NH_3-TPD. [b]The values of Brönsted and Lewis acid sites were calculated from the adsorption of pyridine evacuated at 100 °C.

DOI: 10.1021/acs.energyfuels.9b01649
Energy Fuels 2019, 33, 7726−7737

Brønsted acid sites increased. Also, the intensity of the peaks related to Lewis acid sites increased on increasing the percentage of the Al-HMS(5) matrix in the catalyst.

As shown in Figure 7 and Table 2, the ZAK(35) sample exhibited a higher content of Brönsted acid sites compared with the other hybrid catalysts, and the ratio of Brønsted/Lewis (B/L) acidity was reduced from 2.42 for ZAK(35) to 0.56 for ZAK(15) hybrid catalyst.

3.2. Stability Evaluation. The study of thermal and hydrothermal stability of cracking catalysts is a significant factor because it indicates the operating conditions and the lifetime of the catalyst. In this study, the effect of thermal treatment on the three-component catalyst [ZAK(35)] at different temperatures has been investigated. In a typical experiment, 1.0 g of calcined catalyst (30−50 mesh) was loaded in the middle section of the reactor; this sample was in situ treated at 650 °C under 40 mL min^{-1} flow of dry air for 3 h, and in a similar experiment another sample of ZAK(35) was treated at 750 °C for 3 h under the same condition. After thermal treatment, thermal stability of these samples was evaluated by XRD and BET techniques.

As shown in Figure 8, after thermal treatment at 650 and 750 °C, the typical XRD peaks have been retained for these

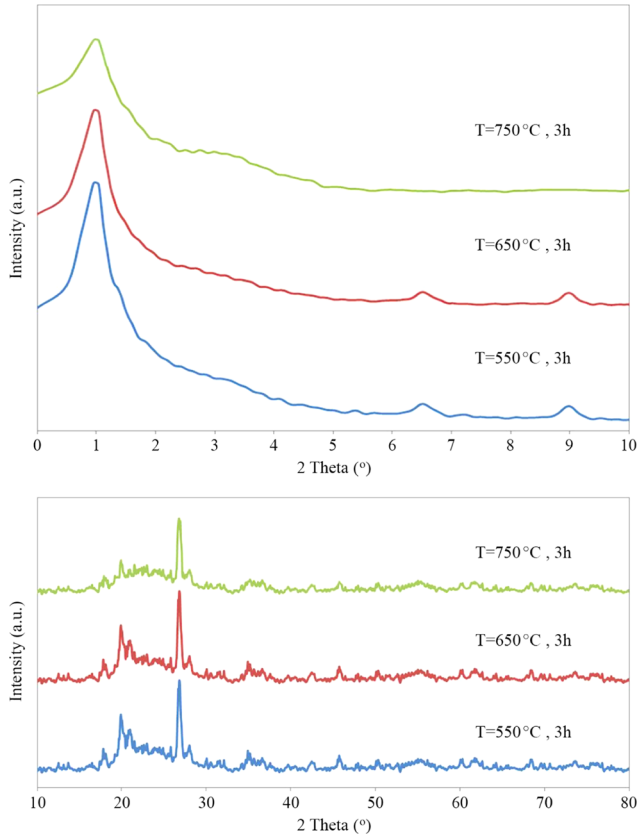

Figure 8. XRD patterns of the ZAK(35) catalyst after thermal treatment at various temperatures for 3 h.

samples; however, on increasing the temperature, the intensity of XRD peaks decreased compared with the sample treated at 550 °C due to reduction of relative crystallinity of these samples and the slight decrease of the framework order. Therefore, these samples exhibit a proper thermal stability, and this result may be due to the presence of Al in the structure of HMS. Several articles have reported that with the substitution of Al in the structure of mesoporous silicates, the strength and stability of these compounds increase.[68−70]

Data presented in Table 3 indicate results of BET analysis for thermal stability evaluation of the ZAK(35) catalyst at various temperatures. As shown in Table 3, the heat treatment at 650 ° C resulted in approximately 8% decrease in the value of the BET surface area compared with the temperature of 550 °C. With a further increase in temperature up to 750 °C, the BET surface area of the catalyst decreased by about 18% and the pore volume of the catalyst did not change significantly. Also, the average pore diameters calculated from the BJH method increased slightly with increasing temperature. Although the values of the BET surface area and pore volume decreased after thermal treatment, the mesoporosity character and shape of the hysteresis loop of the catalyst were well preserved (figure not shown) and the hexagonal array of the Al-HMS channels was not damaged. Therefore, these results indicate that the thermal stability of the catalyst is appropriate and also confirm the results of the XRD test.

Table 3. Results of BET Analysis for the ZAK(35) Catalyst in Thermal Treatment at Various Temperatures[a]

T (°C)	S_{BET} (m^2 g^{-1})	V_{total} (cm^3 g^{-1})	pore size (Å)
550	210	0.23	49
650	193	0.22	51
750	172	0.19	53

[a]Thermal treatment condition: amount of catalyst: 1 g (30−50 mesh); flow of dry air: 40 mL min^{-1}; temperature ramping: 5 °C min^{-1}; time of step at desired temperature (550, 650, and 750 °C): 3 h.

3.3. Catalytic Performance. Catalytic cracking of *n*-hexadecane as a model compound over all of the synthesized catalyst samples was performed to evaluate the catalytic activities of the synthesized two-component (ZA) and three-component (ZAK) catalysts. In the typical test of catalytic cracking, 1.0 g of catalyst (30−50 mesh) and 3.0 g of corundum were loaded in the reactor (Figure 1); after activation, the hexadecane was fed into the reactor along with N_2 carrier gas in a run time of 40 min. The conversion (%), selectivity (%), product yield (%), and carbon balance were calculated according to eqs 1, 2, 3, and 4, respectively. First, two-component (ZA) catalysts were applied in the cracking reaction of *n*-hexadecane to identify the most suitable Si/Al molar ratio in the mesoporous Al-HMS(x) matrix. As mentioned in the experimental section, in two-component (ZA) catalysts, the Al-HMS matrix is containing different Si/Al molar ratios. Table 4 shows the results of these catalytic activity tests. As shown in Table 4, the conversion percentages of *n*-hexadecane over HY-zeolite and HMS are 39 and 10%, respectively. Also, in the presence of the HY/HMS catalyst, conversion (%) changed to 26%. It can be seen that with the addition of HMS to HY-zeolite, the content of the Brönsted acid sites on the hybrid catalyst decreased, which is why the conversion of *n*-hexadecane decreased. According to Table 4, with the participation of Al in the structure of two-component catalysts and decreases of the Si/Al molar ratio in the Al-HMS matrix, first, *n*-hexadecane conversion (%) gradually increases and conversion in the presence of the catalyst HY/Al-HMS(5) (Si/Al = 5) is the maximum value (62.8%), and then conversion decreases with the addition of Al contents. Also, the selectivity of the gasoline product over the HY/Al-HMS(5)

DOI: 10.1021/acs.energyfuels.9b01649
Energy Fuels 2019, 33, 7726−7737

Table 4. Catalytic Cracking of *n*-Hexadecane over the Synthesized Two-Component Catalysts Containing Equal Amounts of Y-Zeolite and Al-HMS Matrix[a]

			selectivity (%)			
catalyst	Si/Al in Al-HMS (molar ratio)	conversion (wt %)	gasoline (C_5–C_{12})	LPG (C_3–C_4)	dry gas (C_1–C_2–CO–CO_2)	coke
HY-zeolite		39.0	50.12	37.44	5.23	7.21
HMS		10.5	28.32	56.68	7.55	7.45
HY/HMS		26.4	53.47	33.07	6.31	7.15
HY/Al-HMS(35)	35	46.7	56.34	28.23	6.98	8.45
HY/Al-HMS(20)	20	50. 5	59.20	25.98	7.48	7.34
HY/Al-HMS(10)	10	57. 4	60.13	26.59	6.52	6.76
HY/Al-HMS(5)	5	62.8	65.78	25.21	3. 34	5.67
HY/Al-HMS(2.5)	2.5	48.9	57.20	31.62	4.86	6.32

[a]Reaction condition: amount of catalyst: 1 g; *n*-hexadecane rate: 4.7 mL h^{-1}; flow of N_2 carrier gas: 140 mL min^{-1}; reaction temperature: 500 °C; run time of each reaction: 40 min. Carbon balance >96% for each run.

catalyst is higher than that of the other catalysts in Table 4, and the same trend that is observed in conversion (%) is also seen in the selectivity of gasoline. In fact, in this series of synthesized catalysts, the ratio of mesopore to microspore structure is constant, and we want to consider the effect of increasing the amount of Al in the mesopores matrix on the catalyst performance. Also, several studies have reported that with the addition of Al to the HMS molecular sieve structure, the acidity of the molecular sieve is increased.[48] From Figure 6A, we can also find that the Al-HMS(5) sample has an NH_3-TPD peak in the range of 200–300 °C, which indicates the acid sites. Therefore, we can conclude that by increasing the amount of Al in the matrix, the acidity of the matrix increased and subsequently the conversion of *n*-hexadecane and selectivity of gasoline increased so that in the presence of the catalyst HY/Al-HMS(5), the conversion of *n*-hexadecane and the selectivity of gasoline are 62 and 65%, respectively. In the HY/Al-HMS(2.5) catalyst, Al introduces a separate phase outside of the HMS structure and may reduce the pore volume and decrease the mesoporosity of the matrix; thus, the conversion and selectivity were reduced. Also, in the XRD pattern of the Al-HMS(2.5) sample, there was severe disorder compared with pure HMS, which confirms this conclusion (not shown in the figure).

In Figure 9, activity of two-component catalysts for gasoline production with respect to the mole of the Al/g matrix is plotted, and a quadratic function for catalyst activity with respect to the mole of the Al/g matrix was observed as follows:

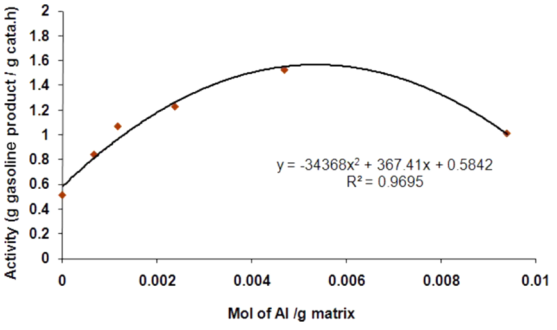

Figure 9. Activity of two-component HY/Al-HMS catalysts in the cracking of *n*-hexadecane as a function of Al loading in the Al-HMS matrix. Reaction conditions: amount of catalyst: 1 g; *n*-hexadecane rate: 4.7 mL h^{-1}; flow of N_2 carrier gas: 140 mL min^{-1}; reaction temperature: 500 °C; run time of each reaction: 40 min. Carbon balance was >96% for each run.

$$Y = -34368X^2 + 367.41X + 0.5842 \quad (5)$$

where X stands for mole of the Al/g matrix and Y is the activity of the catalyst for gasoline production. In fact, these two-component catalysts (ZA) were active in cracking reaction, and activities were increased with Al loadings. However, on the other hand, there was a limitation on the diffusion of materials through the catalyst structure channels, and this limitation also gradually increased with Al loading in the HMS. There was also a limitation on the increase of the acidity of the HMS. Therefore, the catalytic activity increased to some extent, and then its amount decreased due to the effect of limitation of diffusion and reduction of acidity.

The HY/Al-HMS(5) catalyst has a higher conversion for the hexadecane cracking process among the synthesized two-component catalysts. Therefore, HY/Al-HMS(5) may be a better catalyst, and Al-HMS(5) (with Si/Al = 5) was selected as a proper matrix to prepare the three-component (ZAK) catalysts.

In the second step, by investigating the types and amounts of components of conventional catalysts in the FCC process, NH_4Y-zeolite and Al-HMS(5) matrix were combined with 50 wt % clay K10 as a filler (Section 2), and the three-component catalysts (ZAK(x)) (x represents the weight percentage of NH_4Y-zeolite) were applied in the cracking reaction of *n*-hexadecane. The results of these catalytic performance tests are shown in Table 5. According to Table 5, in the ZAK catalysts, with increase in the percentage of zeolite content from 15 to 35%, the *n*-hexadecane conversion increased from 59 to 69%, respectively. Also, the selectivity of gasoline increased from 57% for ZAK(15) to 71% for ZAK(35), and the selectivity of the LPG product decreased slightly from 28% for ZAK(15) to 20% for the catalyst ZAK(35). Also, the selectivity of dry gas and coke formation also decreased.

From Figure 2B it can be found that the components of catalysts ZAK are well combined and the lattice disorder of the matrix Al-HMS(5) increased from interaction with the HY-zeolite component. Also, from Table 1 it can be concluded that by increasing the matrix, the relative crystallinity (R.C.) parameters of the ZAK catalysts were reduced compared with those of pure zeolite due to the interaction with the Al-HMS matrix so that R.C. decreased from 58.2 for ZAK(35) to 35.2 for ZAK(15). It is clear from Figure 3 that ZAK(x) samples display type I–IV isotherms with mesoporous characteristics and highly uniform cylindrical pores; from Table 1 it can be found that the pore diameter values of ZAK catalysts increased slightly with increasing zeolite content and the ratio of V_{meso}/

DOI: 10.1021/acs.energyfuels.9b01649
Energy Fuels 2019, 33, 7726–7737

Table 5. Catalytic Cracking of *n*-Hexadecane over the Three-Component Catalysts ZAK(x) Containing 50 wt % Clay K10, x wt % Y-Zeolite, and (50 − x) wt % Al-HMS(5) Matrix[a]

		selectivity (%)				
catalyst	conversion (wt %)	gasoline (C_5–C_{12})	LPG (C_3–C_4)	dry gas (C_1–C_2–CO–CO_2)	coke (%)	ON[b]
ZAK(15)	59.7	57.84	28.50	7.32	6.34	87.23
ZAK(25)	65.3	68.21	20.66	5. 79	5.34	88.46
ZAK(35)	69.5	71.47	20.19	4.56	3.78	89.14

[a]Reaction condition: amount of catalyst: 1 g; *n*-hexadecane rate, 4.7 mL h^{-1}; flow of N_2 carrier gas: 140 mL min^{-1}; reaction temperature: 500 °C; run time of each reaction: 40 min. Carbon balance was >96% for each run. [b]Gasoline octane number (ON) was calculated from the equation $ON = \sum V_i B_i^{ON}$.

V_{micro} increased from 4.75 for ZAK(15) to 8.58 for ZAK(35). From the NH_3-TPD experiment (Figure 6), FTIR-pyridine spectra (Figure 7), and Table 2, the Brønsted/Lewis acid site ratio increased from 0.56 for ZAK(15) to 2.42 for ZAK(35). As mentioned before, from NH_3-TPD profiles of the ZAK(35) catalyst, it can be found that this sample contains moderate to strong acid sites and the content of superstrong acidic sites is lower than that of ZAK(25) and ZAK(15) samples; additionally, it produced more gasoline yield and less dry gas and coke. Therefore, ZAK(35) is a desirable catalyst for this reaction. In fact, an increase in NH_4-Y-zeolite content from 15 to 35% produces significant changes in textural properties, phase composition, morphology, Brønsted/Lewis acid sites ratios, and relative contents of meso-/micropores of the ZAK catalysts. In fact, such changes in the structural properties of the catalyst have led to these observed differences in catalytic efficiency. Therefore, it seems that catalyst ZAK(35) among the three-component catalysts in Table 5 is a suitable catalyst for *n*-hexadecane cracking reaction. Also, the last column of Table 5 shows the octane numbers of gasoline produced in this experiment, which are appropriate values for the liquid fuel. Octane number depends on the molecular structure and carbon number of the hydrocarbon components in the gasoline product. The gasoline octane number (ON) was calculated using the following equation:

$$\mathrm{ON} = \sum V_i B_i^{ON} \tag{6}$$

where V_i is the volume fraction of the ith component of the gasoline, and B_i^{ON} is the contribution of the ith component to creating the octane number of fuels. The B_i^{ON} values are taken from the literature.[71]

Data from Table 5 was used, and Figure 10 was drawn. In Figure 10, the conversion (%) of *n*-hexadecane and the yield (%) of products are shown for catalysts ZAK with different Y-zeolite contents. As shown in Figure 10, catalyst ZAK(35) has the highest percentage of conversion, and the yield of gasoline increased from 34% for ZAK(15) to 49% for ZAK(35).

3.3.1. Effect of Reaction Temperature. Figure 11 shows the changes of conversion (%) and yields of products in the cracking of *n*-hexadecane over the ZAK(35) catalyst at reaction temperatures of 450, 500, and 550 °C. The reaction rate depends on temperature because rate constant is an exponential function of temperature, and usually conversion (%) increases with increasing reaction temperature. In Figure 11, with a 50 °C increase of temperature, the conversion (%) shifted from 69 to 76%, which it has increased by 10%. However, the yield (%) decreased for gasoline and increased for LPG and dry gas. Therefore, the temperature of 500 °C is proper for the cracking of *n*-hexadecane over the ZAK(35) catalyst.

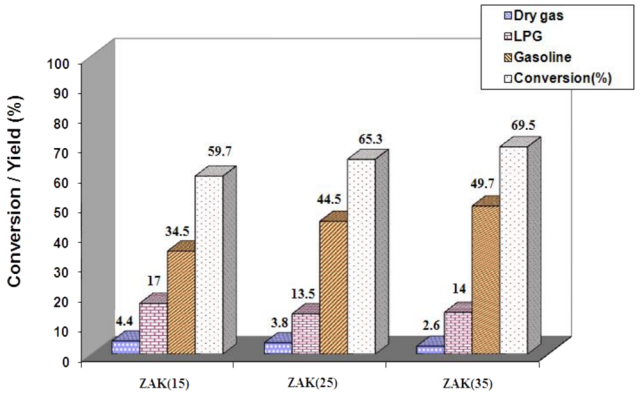

Figure 10. Conversion of *n*-hexadecane and yields of reaction products over ZAK(15), ZAK(25), and ZAK(35) catalysts with various loadings of Y-zeolite. Reaction conditions: amount of catalyst: 1 g; *n*-hexadecane rate: 4.7 mL h^{-1}; flow of N_2 carrier gas: 140 mL min^{-1}; reaction temperature: 500 °C; run time of each reaction: 40 min. Carbon balance was >96% for each run.

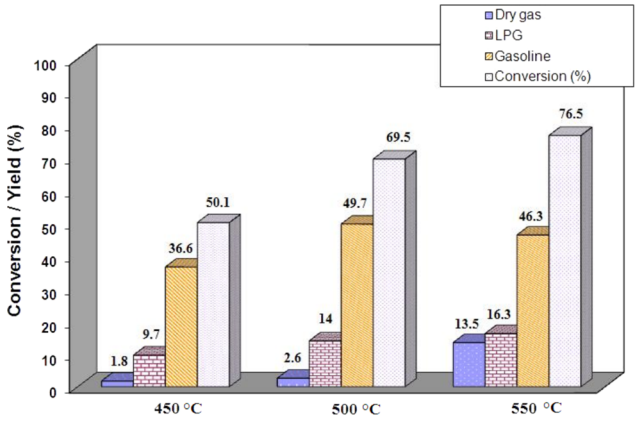

Figure 11. Conversion of *n*-hexadecane and yields of products in the cracking of *n*-hexadecane over the ZAK(35) catalyst at various reaction temperatures. Reaction conditions: amount of catalyst: 1 g; *n*-hexadecane rate: 4.7 mL h^{-1}; flow of N_2 carrier gas: 140 mL min^{-1}; reaction temperature; 500 °C; run time of each reaction: 40 min. Carbon balance was >96% for each run.

4. CONCLUSIONS

Briefly, an Al-HMS molecular sieve with different Si/Al molar ratios and faujasite-type HY-zeolite was successfully synthesized and combined with an equal weight ratio, and for the first time, their catalytic activities were evaluated for *n*-hexadecane cracking reaction to identify the most suitable Si/Al molar ratio in the mesoporous Al-HMS matrix. These experiments showed that with the incorporation of Al in the HMS molecular sieve structure, the acidity of the molecular sieve increased and the

DOI: 10.1021/acs.energyfuels.9b01649
Energy Fuels 2019, 33, 7726−7737

ratio of Si/Al = 5 in the matrix structure is more appropriate. In the presence of the catalyst HY/Al-HMS(5), the conversion of *n*-hexadecane and the selectivity of gasoline are 62 and 65%, respectively. For these two-component catalysts, a quadratic function for catalyst activity with respect to the mole of the Al/g matrix was observed. In the second step, various amounts of faujasite-type HY-zeolite and Al-HMS(5) matrix were combined with the montmorillonite K10 as a filler to prepare the three-component catalysts (ZAK). These catalyst samples were also applied in the cracking reaction of *n*-hexadecane. These experiments showed that the three-component catalysts ZAK(35) with content of 50 wt % montmorillonite K10, 35 wt % NH_4Y-zeolite, and 15 wt % Al-HMS(5) gave the best efficiency with 69% conversion of *n*-hexadecane, 71% selectivity of gasoline, and 20% selectivity of dry gas with gasoline octane number of 89.14. In fact, hybrid catalyst ZAK(35) with appropriate combination of mesoporous and microporous characters and high Brønsted/Lewis acid sites ratio is an efficient catalyst for this cracking reaction.

AUTHOR INFORMATION

Corresponding Author

*E-mail: v-mahdavi@araku.ac.ir. Fax: +98 863 4173406.

ORCID

Vahid Mahdavi: 0000-0001-5823-5628

Notes

The authors declare no competing financial interest.

ACKNOWLEDGMENTS

This work was supported by the Shazand Oil Refinery, Arak, Iran, so the authors sincerely thank the research council of this company.

REFERENCES

(1) Sadeghbeigi, R. *Fluid Catalytic Cracking: Design, Operation, and Troubleshooting of FCC Facilities*; Gulf Publishing Company: Houston, 2000.

(2) Hosseinpour, N.; Mortazavi, Y.; Bazyari, A.; Khodadadi, A. Synergetic effects of Y-zeolite and amorphous silica-alumina as main FCC catalyst components on triisopropylbenzene cracking and coke formation. *Fuel Process. Technol.* **2009**, *90*, 171−179.

(3) Hosseinpour, N.; Khodadadi, A. A.; Mortazavi, Y.; Bazyari, A. Nano-ceria−zirconia promoter effects on enhanced coke combustion and oxidation of CO formed in regeneration of silica−alumina coked during cracking of triisopropylbenzene. *Appl. Catal., A* **2009**, *353*, 271−281.

(4) Rase, H. F. *Handbook of Commercial Catalysts: Heterogeneous Catalysts*; CRC Press, 2016.

(5) Rana, M. S.; Samano, V.; Ancheyta, J.; Diaz, J. A review of recent advances on process technologies for upgrading of heavy oils and residua. *Fuel* **2007**, *86*, 1216−1231.

(6) Andreu, P. Development of catalysts for the fluid catalytic cracking process: an example of CYTED-D program. *Catal. Lett.* **1993**, *22*, 135−146.

(7) Wallenstein, D.; Harding, R. The dependence of ZSM-5 additive performance on the hydrogen-transfer activity of the REUSY base catalyst in fluid catalytic cracking. *Appl. Catal., A* **2001**, *214*, 11−29.

(8) Liu, H.; Zhao, H.; Gao, X.; Ma, J. A novel FCC catalyst synthesized via in situ overgrowth of NaY zeolite on kaolin microspheres for maximizing propylene yield. *Catal. Today* **2007**, *125*, 163−168.

(9) He, L.-J.; Zheng, S.-Q.; Dai, Y.-L. An FCC Catalyst for Maximizing Gasoline Yield. *Kem. Ind.* **2017**, *66*, 9−15.

(10) Qi, J.; Jin, Q.; Zhao, K.; Zhao, T. Catalytic cracking of 1,3,5-triisopropylbenzene over silicoaluminophosphate with hierarchical pore structure. *J. Porous Mater.* **2015**, *22*, 1021−1032.

(11) Qiu, S.; Xue, M.; Zhu, G. Metal−organic framework membranes: from synthesis to separation application. *Chem. Soc. Rev.* **2014**, *43*, 6116−6140.

(12) Pires, J.; Carvalho, A.; de Carvalho, M. B. Adsorption of volatile organic compounds in Y zeolites and pillared clays. *Microporous Mesoporous Mater.* **2001**, *43*, 277−287.

(13) Cundy, C. S.; Cox, P. A. The hydrothermal synthesis of zeolites: history and development from the earliest days to the present time. *Chem. Rev.* **2003**, *103*, 663−702.

(14) Marcilly, C. *Acido-Basic Catalysis: Application to Refining and Petrochemistry*; Technip & Ophrys Editions, 2006; Vol. *2*.

(15) Katada, N.; Niwa, M. Analysis of acidic properties of zeolitic and non-zeolitic solid acid catalysts using temperature-programmed desorption of ammonia. *Catal. Surv. Asia* **2004**, *8*, 161−170.

(16) Peng, L.; Chupas, P. J.; Grey, C. P. Measuring brønsted acid densites in zeolite HY with diphosphine molecules and solid state NMR spectroscopy. *J. Am. Chem. Soc.* **2004**, *126*, 12254−12255.

(17) Gulzira, V.; Raisa, M.; Elmira, Y.; Zhaksyntay, K. The Influence of Mechanochemical Treatment on the Acid and Catalytic Properties of Modified Natural Zeolite. *Adv. Mater. Res.* **2012**, 2127−2130.

(18) Teyssier, L.; Thomas, M.; Bouchy, C.; Martens, J.; Guillon, E. Liquid chromatography method for quantification of surface connected mesoporosity in ultrastable Y zeolites. *Microporous Mesoporous Mater.* **2007**, *100*, 6−11.

(19) Xiong, K.; Lu, C.; Wang, Z.; Gao, X. Kinetic study of catalytic cracking of heavy oil over an in-situ crystallized FCC catalyst. *Fuel* **2015**, *142*, 65−72.

(20) Groen, J. C.; Moulijn, J. A.; Pérez-Ramírez, J. Desilication: on the controlled generation of mesoporosity in MFI zeolites. *J. Mater. Chem.* **2006**, *16*, 2121−2131.

(21) Al-Shammari, A. A.; Ali, S. A.; Al-Yassir, N.; Aitani, A. M.; Ogunronbi, K. E.; Al-Majnouni, K. A.; Al-Khattaf, S. S. Catalytic cracking of heavy naphtha-range hydrocarbons over different zeolites structures. *Fuel Process. Technol.* **2014**, *122*, 12−22.

(22) Hosseinpour, N.; Mortazavi, Y.; Khodadadi, A. A. Cumene cracking activity and enhanced regeneration of FCC catalysts comprising HY-zeolite and $LaBO_3$ (B = Co, Mn, and Fe) perovskites. *Appl. Catal., A* **2014**, *487*, 26−35.

(23) Feng, R.; Yan, X.; Hu, X.; Qiao, K.; Yan, Z.; Rood, M. J. High performance of H_3BO_3 modified USY and equilibrium catalyst with tailored acid sites in catalytic cracking. *Microporous Mesoporous Mater.* **2017**, *243*, 319−330.

(24) Weckhuysen, B. M.; Yu, J. Recent advances in zeolite chemistry and catalysis. *Chem. Soc. Rev.* **2015**, *44*, 7022−7024.

(25) Venuto, P.; Habib, T. Catalyst-feedstock-engineering interactions in fluid catalytic cracking. *Catal. Rev.* **1978**, *18*, 1−150.

(26) Jiao, W.; Wu, X.; Li, G.; Xue, T.; Wang, Y.; Tang, Y. Core−Shell Zeolite Y@ γ-Al_2O_3 Nanorod Composites: Optimized Fluid Catalytic Cracking Catalyst Assembly for Processing Heavy Oil. *ChemCatChem* **2017**, *9*, 2574−2583.

(27) Corma, A.; Martínez, C.; Sauvanaud, L. New materials as FCC active matrix components for maximizing diesel (light cycle oil, LCO) and minimizing its aromatic content. *Catal. Today* **2007**, *127*, 3−16.

(28) Ishihara, A.; Kimura, K.; Owaki, A.; Inui, K.; Hashimoto, T.; Nasu, H. Catalytic cracking of VGO by hierarchical ZSM-5 zeolite containing mesoporous silica−aluminas using a Curie point pyrolyzer. *Catal. Commun.* **2012**, *28*, 163−167.

(29) Maselli, J. M.; Peters, A. W. Preparation and Properties of Fluid Cracking Catalysts for Residual Oil Conversion. *Catal. Rev.* **1984**, *26*, 525−554.

(30) Zheng, J.; Zhang, H.; Liu, Y.; Wang, G.; Kong, Q.; Pan, M.; Tian, H.; Li, R. Synthesis of Wool-Ball-Like ZSM-5 with Enlarged External Surfaces and Improved Diffusion: A Potential Highly-Efficient FCC Catalyst Component for Elevating Pre-cracking of Large Molecules and Catalytic Longevity. *Catal. Lett.* **2016**, *146*, 1457−1469.

DOI: 10.1021/acs.energyfuels.9b01649
Energy Fuels 2019, 33, 7726−7737

(31) Zhang, Q.; Li, C.; Xu, S.; Shan, H.; Yang, C. Synthesis of a ZSM-5(core)/SAPO-5(shell) composite and its application in FCC. *J. Porous Mater.* **2013**, *20*, 171−176.
(32) Jia, L.; Sun, X.; Ye, X.; Zou, C.; Gu, H.; Huang, Y.; Niu, G.; Zhao, D. Core−shell composites of USY@Mesosilica: Synthesis and application in cracking heavy molecules with high liquid yield. *Microporous Mesoporous Mater.* **2013**, *176*, 16−24.
(33) Meng, Q.; Liu, B.; Piao, J.; Liu, Q. Synthesis of the composite material Y/ASA and its catalytic performance for the cracking of n-decane. *J. Catal.* **2012**, *290*, 55−64.
(34) Waller, P.; Shan, Z.; Marchese, L.; Tartaglione, G.; Zhou, W.; Jansen, J. C.; Maschmeyer, T. Zeolite nanocrystals inside mesoporous TUD-1: A high-performance catalytic composite. *Chem. − Eur. J.* **2004**, *10*, 4970−4976.
(35) Hamdy, M. S.; Mul, G. TUD-1-Encapsulated HY Zeolite: A New Hierarchical Microporous/Mesoporous Composite with Extraordinary Performance in Benzylation Reactions. *ChemCatChem* **2013**, *5*, 3156−3163.
(36) Beck, J. S.; Vartuli, J. C.; Roth, W. J.; Leonowicz, M. E.; Kresge, C. T.; Schmitt, K. D.; Chu, C. T. W.; Olson, D. H.; Sheppard, E. W.; McCullen, S. B.; et al. A new family of mesoporous molecular sieves prepared with liquid crystal templates. *J. Am. Chem. Soc.* **1992**, *114*, 10834−10843.
(37) Kresge, C.; Leonowicz, M.; Roth, W. J.; Vartuli, J.; Beck, J. Ordered mesoporous molecular sieves synthesized by a liquid-crystal template mechanism. *Nature* **1992**, *359*, 710.
(38) van Donk, S.; Janssen, A. H.; Bitter, J. H.; de Jong, K. P. Generation, Characterization, and Impact of Mesopores in Zeolite Catalysts. *Catal. Rev.* **2003**, *45*, 297−319.
(39) Mahdavi, V.; Mardani, M.; Malekhosseini, M. Oxidation of alcohols with tert-butylhydroperoxide catalyzed by Mn (II) complexes immobilized in the pore channels of mesoporous hexagonal molecular sieves (HMS). *Catal. Commun.* **2008**, *9*, 2201−2204.
(40) Mahdavi, V.; Hasheminasab, H. R.; Abdollahi, S. Liquid phase selective oxidation of alcohols over VPO catalysts supported on mesoporous Hexagonal Molecular Sieves (HMS). *J. Chin. Chem. Soc.* **2010**, *57*, 189−198.
(41) Yin, A.; Qu, J.; Guo, X.; Dai, W.-L.; Fan, K. The influence of B-doping on the catalytic performance of Cu/HMS catalyst for the hydrogenation of dimethyloxalate. *Appl. Catal., A* **2011**, *400*, 39−47.
(42) Zhang, P.; Ma, X. Catalytic synthesis of diethyl carbonate by oxidative carbonylation of ethanol over $PdCl_2$/Cu-HMS catalyst. *Chem. Eng. J.* **2010**, *163*, 93−97.
(43) Kosslick, H.; Lischke, G.; Walther, G.; Storek, W.; Martin, A.; Fricke, R. Physico-chemical and catalytic properties of Al-, Ga-and Fe-substituted mesoporous materials related to MCM-41. *Microporous Mater.* **1997**, *9*, 13−33.
(44) Occelli, M.; Biz, S.; Auroux, A. Effects of isomorphous substitution of Si with Ti and Zr in mesoporous silicates with the MCM-41 structure. *Appl. Catal., A* **1999**, *183*, 231−239.
(45) Lin, H.-Y.; Pan, Y.-L.; Chen, Y.-W. Characteristics of gallium-substituted hexagonal mesoporous silica: effects of gallium content. *J. Porous Mater.* **2005**, *12*, 151−164.
(46) Bhoware, S. S.; Shylesh, S.; Kamble, K.; Singh, A. Cobalt-containing hexagonal mesoporous molecular sieves (Co-HMS): Synthesis, characterization and catalytic activity in the oxidation reaction of ethylbenzene. *J. Mol. Catal. A: Chem.* **2006**, *255*, 123−130.
(47) Reddy, J. S.; Sayari, A. Room-temperature synthesis of a highly active vanadium-containing mesoporous molecular sieve, V-HMS. *J. Chem. Soc., Chem. Commun.* **1995**, *21*, 2231−2232.
(48) Chiranjeevi, T.; Kumaran, G. M.; Gupta, J.; Dhar, G. M. Synthesis and characterization of acidic properties of Al-HMS materials of varying Si/Al ratios. *Thermochim. Acta* **2006**, *443*, 87−92.
(49) Hamoule, T.; Peyrovi, M.; Rashidzadeh, M.; Toosi, M. Catalytic reforming of n-heptane over Pt/Al-HMS catalysts. *Catal. Commun.* **2011**, *16*, 234−239.
(50) Kulikov, A.; Pugacheva, A.; Maksimov, A. Modified mesoporous catalysts based on Al-HMS and Al-MCF for the oligomerization of α-olefins. *Pet. Chem.* **2014**, *54*, 426−430.
(51) Onaka, M.; Hashimoto, N.; Kitabata, Y.; Yamasaki, R. Aluminum-rich mesoporous aluminosilicate (Al-HMS) as a solid acid catalyst for the Diels−Alder reaction of acrylates with 1,3-dienes. *Appl. Catal., A* **2003**, *241*, 307−317.
(52) Robson, H. *Verified Synthesis of Zeolitic Materials*; Gulf Professional Publishing, 2001.
(53) Tanev, P. T.; Pinnavaia, T. J. A neutral templating route to mesoporous molecular sieves. *Science* **1995**, *267*, 865−867.
(54) Mokaya, R.; Jones, W. Physicochemical characterisation and catalytic activity of primary amine templated aluminosilicate mesoporous catalysts. *J. Catal.* **1997**, *172*, 211−221.
(55) Mahdavi, V.; Monajemi, A. Gas phase dehydration of glycerol catalyzed by gamma Al_2O_3 supported V_2O_5: a statistical approach for simultaneous optimization. *RSC Adv.* **2016**, *6*, No. 114244.
(56) Miyazawa, K.; Inagaki, S. Control of the microporosity within the pore walls of ordered mesoporous silica SBA-15. *Chem. Commun.* **2000**, *21*, 2121−2122.
(57) Bazyari, A.; Khodadadi, A.; Hosseinpour, N.; Mortazavi, Y. Effects of steaming-made changes in physicochemical properties of Y-zeolite on cracking of bulky 1,3,5-triisopropylbenzene and coke formation. *Fuel Process. Technol.* **2009**, *90*, 1226−1233.
(58) He, L.; Zheng, S.; Ren, S.; Yu, H.-X.; Zhang, J.-c. New resid FCC catalyst for maximizing gasoline yield. *Pet. Chem.* **2017**, *57*, 60−65.
(59) Guth, J.-L.; Kessler, H. Synthesis of Aluminosilicate Zeolites and Related Silica-Based Materials. *Catalysis and Zeolites*; Springer, 1999; pp 1−52.
(60) Zhou, J.; Liu, Z.; Wang, Y.; Gao, H.; Li, L.; Yang, W.; Xie, Z.; Tang, Y. Enhanced accessibility and utilization efficiency of acid sites in hierarchical MFI zeolite catalyst for effective diffusivity improvement. *RSC Adv.* **2014**, *4*, 43752−43755.
(61) Parsafard, N.; Peyrovi, M.; Jarayedi, M. Catalytic study and kinetic modeling of the n-heptane isomerization over Pt/Al-HMS/HZSM-5 hybrid catalysts. *Energy Fuels* **2017**, *31*, 6389−6396.
(62) Karge, H. Characterization by infrared spectroscopy. *Microporous Mesoporous Mater.* **1998**, *22*, 547−549.
(63) Liu, X. DRIFTS study of surface of γ-alumina and its dehydroxylation. *J. Phys. Chem. C* **2008**, *112*, 5066−5073.
(64) Peyrovi, M. H.; Hamoule, T. Study of catalytic properties of Pt/Al-HMS catalysts in n-heptane hydroisomerization. *React. Kinet., Mech. Catal.* **2012**, *106*, 233−243.
(65) Yin, A.; Guo, X.; Dai, W.-L.; Fan, K. Effect of Si/Al Ratio of mesoporous support on the structure evolution and catalytic performance of the Cu/Al-HMS catalyst. *J. Phys. Chem. C* **2010**, *114*, 8523−8532.
(66) Yu, W.; Zhou, C.; Lue, D.; Zhang, B.; Xu, X. Synthesis and characterization of Al-HMS catalysts and their application for t-butylation of toluene. *Indian J. Chem., Sect. A: Inorg., Phys., Theor. Anal.* **2008**, *47*, 181−185.
(67) Ardagh, M. A.; Bo, Z.; Nauert, S. L.; Notestein, J. M. Depositing SiO_2 on Al_2O_3: a route to tunable Brønsted acid catalysts. *ACS Catal.* **2016**, *6*, 6156−6164.
(68) Tang, Y.; Chen, Y.; Wu, Y.; Zheng, M.; Zhang, C.; Yang, M.; Cao, G. Production of mesoporous materials with high hydrothermal stability by doping metal heteroatoms. *Microporous Mesoporous Mater.* **2016**, *224*, 420−425.
(69) Mayanovic, R. A.; Yan, H.; Brandt, A. D.; Wang, Z.; Mandal, M.; Landskron, K.; Bassett, W. A. Mechanical and hydrothermal stability of mesoporous materials at extreme conditions. *Microporous Mesoporous Mater.* **2014**, *195*, 161−166.
(70) Liu, Y.; Pinnavaia, T. J. Aluminosilicate mesostructures with improved acidity and hydrothermal stability. *J. Mater. Chem.* **2002**, *12*, 3179−3190.
(71) Ghosh, P.; Hickey, K. J.; Jaffe, S. B. Development of a detailed gasoline composition-based octane model. *Ind. Eng. Chem. Res.* **2006**, *45*, 337−345.

DOI: 10.1021/acs.energyfuels.9b01649
Energy Fuels 2019, 33, 7726−7737